Microtubule motors involved in nuclear movement during skeletal muscle differentiation

V. Gache[a,†], E. R. Gomes[a,b,*], and B. Cadot[a,*]
[a]Center of Research in Myology, INSERM UPMC UMR974, Centre National de la Recherche Scientifique, FRE3617, 75013 Paris, France; [b]Instituto de Medicina Molecular, Faculdade de Medicina da Universidade de Lisboa, 1649-028 Lisbon, Portugal

ABSTRACT **Nuclear positioning is a determining event in several cellular processes, such as fertilization, cell migration, and cell differentiation. The structure and function of muscle cells, which contain hundreds of nuclei, have been shown to rely in part on proper nuclear positioning. Remarkably, in the course of muscle differentiation, nuclear movements along the myotube axis might represent the event required for the even positioning of nuclei in the mature myofiber. Here we analyze nuclear behavior, time in motion, speed, and alignment during myotube differentiation and temporal interference of cytoskeletal microtubule-related motors. Using specific inhibitors, we find that nuclear movement and alignment are microtubule dependent, with 19 microtubule motor proteins implicated in at least one nuclear behavior. We further focus on Kif1c, Kif5b, kif9, kif21b, and Kif1a, which affect nuclear alignment. These results emphasize the different roles of molecular motors in particular mechanisms.**

Monitoring Editor
Laurent Blanchoin
CEA Grenoble

Received: Jun 14, 2016
Revised: Feb 1, 2017
Accepted: Feb 1, 2017

INTRODUCTION

The skeletal muscle fiber is a syncytium resulting from the fusion of hundreds of myoblasts (Abmayr and Pavlath, 2012). Muscle cells represent the main vertebrate cell type and are specialized to contract, and thus are responsible for voluntary movements. During muscle development or regeneration, nuclei are first found in the center of myotubes and then migrate to the periphery of mature skeletal myofibers (Bruusgaard *et al.*, 2003). Proper nuclear positioning is required for muscle function (Metzger *et al.*, 2012), and nuclear mispositioning is a hallmark of different muscle disorders, such as centronuclear myopathies (Jungbluth *et al.*, 2008).

Multiple nuclear movement events occur during myofiber development to localize precisely each individual nucleus (Cadot *et al.*, 2012; Metzger *et al.*, 2012; Wilson and Holzbaur, 2012, 2015; Falcone *et al.*, 2014). The first nuclear migration event in muscle development takes place just after fusion, when the nucleus from a fusing myoblast rapidly migrates toward the center of the myotube. This process is called centration (Cadot *et al.*, 2012). Second, nuclei spread to become evenly spaced along the length of developing myotubes (Metzger *et al.*, 2012), a step called spreading. These two events were proposed to rely on the microtubule (MT) network and on some motor proteins. Finally, as myotubes mature into myofibers, nuclei migrate from the center to the periphery of the fiber by a mechanism dependent on N-Wasp, an actin regulator, and amphiphysin-2, a BAR protein mutated in centronuclear myopathies. This nuclear migration is termed dispersion (Falcone *et al.*, 2014). Nuclear positioning in cells appears to be a key mechanism required for multiple developmental processes in order to maintain functionally efficient muscle or brain (Dauer and Worman, 2009). These processes are described as being driven by MTs or actin (Gundersen and Worman, 2013). Even though recent advances in understanding nuclei position in developing muscle cells reveal an important role of MTs and some MT motors (kinesins and dyneins; Cadot *et al.*, 2012; Metzger *et al.*, 2012; Wilson and Holzbaur, 2012), the contribution of other MT motors to nuclei position during myofiber formation remains unexplored.

This article was published online ahead of print in MBoC in Press (http://www.molbiolcell.org/cgi/doi/10.1091/mbc.E16-06-0405) on February 8, 2017.

V.G., E.R.G., and B.C. conceived and designed the experiments; V.G. and B.C. performed the experiments; V.G. and B.C. analyzed the data; V.G., E.R.G., and B.C. drafted the article; B.C. prepared the digital images.

[†]Present address: Institut NeuroMyogène, CNRS UMR 5310, INSERM U1217, Université de Lyon, Ecole Normale Supérieure de Lyon, 69364 Lyon Cedex 07, France.

*Address correspondence to: E. R. Gomes (edgargomes@medicina.ulisboa.pt), B. Cadot (bruno.cadot@upmc.fr).

Abbreviations used: GFP, green fluorescent protein; MT, microtubules; siRNA, small interfering RNA.

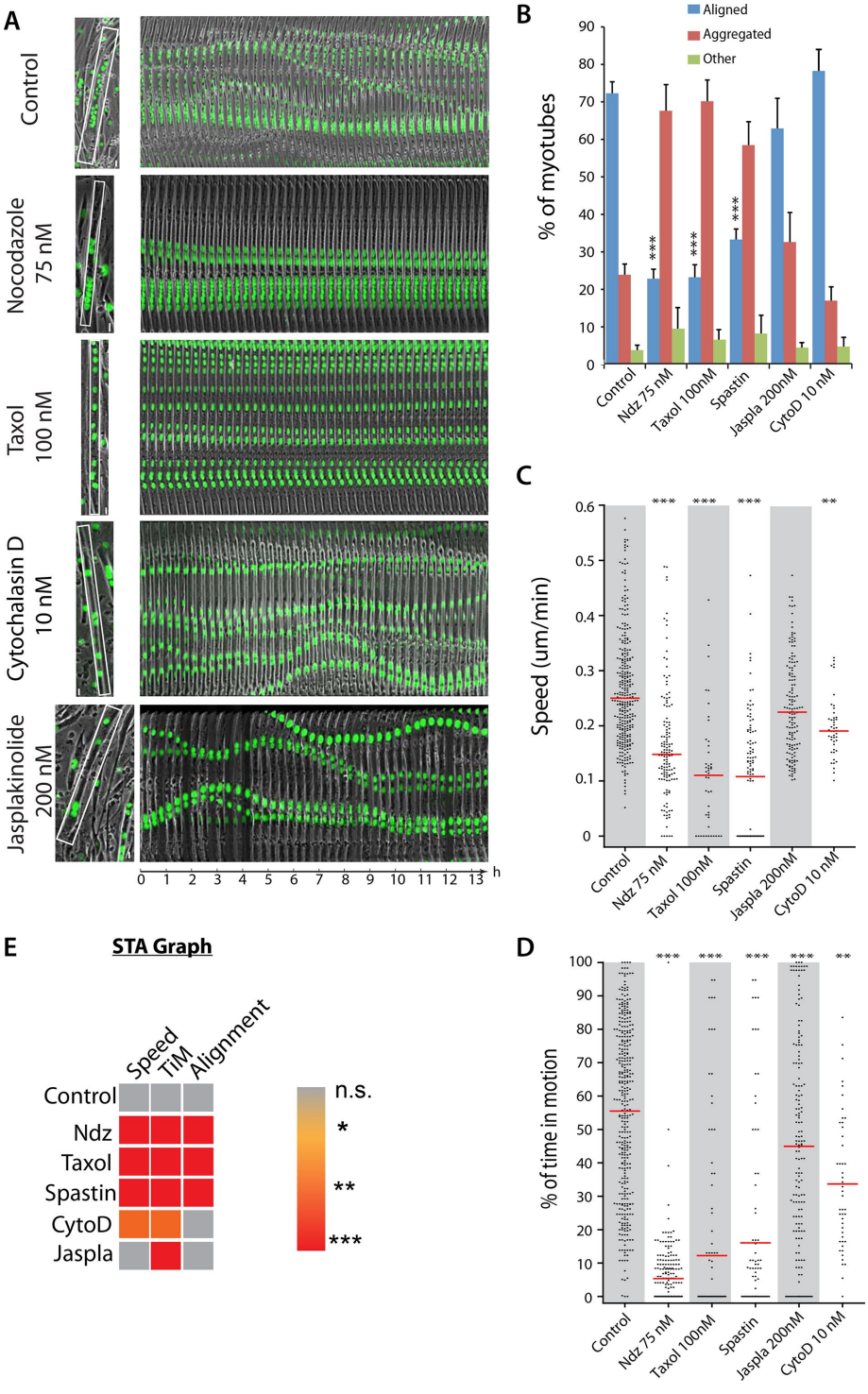

FIGURE 1: Role of MTs and actin in nuclear movement inside myotubes. (A) Frames from time-lapse two-channel movies (phase contrast and fluorescence) of differentiated GFP-H1-C2 cells in presence or absence of the indicated drugs (Supplemental Movie S1). The first frame of each representative 14-h movie shows a myotube with GFP-H1-C2 nuclei (green); the white rectangle corresponds to the region used to create the adjacent kymograph. (B) Histogram of nuclear distribution analysis in C2C12 myotubes: nontreated (Control), treated with 75 nM nocodazole (Ndz), 100 nM Taxol (Taxol), 200 nM jasplakinolide (Jaspla), or 10 nM cytochalasin D (CytoD), or transfected with GFP-spastin. Nuclear distribution is quantified as "aligned" if >70% of nuclei are aligned along the same axis; "aggregated" if >70% of nuclei do not align along the same axis; and "other" if nuclei are both aggregated and aligned in the same myotube. (C) Speed and (D) percentage of time in motion of nuclei inside C2C12 myotubes 2–3 d old in nontreated (Control), treated with 75 nM Ndz, 100 nM Taxol, 200 nM Jaspla, or 10 nM CytoD conditions or transfected with GFP-spastin. Red line indicates the median. Between 53 (CytoD) and 181 (Ctr) nuclei were monitored from three different experiments. Error bars, SEM. ***$p < 0.001$, **$p < 0.01$. (E) STA graph; color is representative of the p value after one-way analysis of variance (ANOVA) statistical test toward a decrease compared to control. ***$p < 0.001$, **$p < 0.01$, *$p < 0.05$.

Here we present a comprehensive analysis of MT-related molecular motor involvement in nuclear spreading during myofiber development. We use time-lapse microscopy combined with a small interfering RNA (siRNA) screen targeting all MT-related molecular motors (kinesins and dyneins) of the mouse genome to identify their involvement. These results highlight the variable effects of molecular motors on particular mechanisms in the early phases of myofiber development, such as nuclear alignment, time in motion, and speed of nuclei inside myotubes.

RESULTS AND DISCUSSION

Nuclear movements contribute to nuclei alignment inside myotubes

Nuclear movements occur in both primary differentiated muscle cells and C2C12s (Figure 1A; Englander and Rubin, 1987; Cadot *et al.*, 2012; Metzger *et al.*, 2012; Wilson and Holzbaur, 2012). We therefore used C2C12 muscle cells (Cadot *et al.*, 2012), stably expressing green fluorescent protein (GFP)–histone H1, to quantify nuclear behaviors during myotube formation using time-lapse microscopy. Nuclei within myotubes follow different behaviors, suggesting that multiple forces are applied to nuclei, driving their displacement along developing myofibers. To better characterize these nuclear migrations, we tracked each nucleus inside myotubes during the first 4 d of myofiber development and analyzed nuclear movements using SkyPad (Cadot *et al.*, 2014) to extract speed and percentage of time in motion. We also quantified nuclei distribution in myotubes to measure whether the resulting forces on each nucleus lead to a "nuclei alignment" organization (Metzger *et al.*, 2012). Finally, we analyzed fusion index to correlate defects in nuclear behavior with differentiation. During differentiation, nuclei progressively reduce their movements (Supplemental Figure S1A), and after 4 d, nuclei are mostly spread along the myotube axis (Figures 1B and 2C; Metzger *et al.*, 2012). Reduction of speed and time in motion during differentiation suggests that nuclear movement is not driven by a unique mechanism. We therefore decided to perform our analysis of nuclear movement between 60 and 75 h of differentiation,

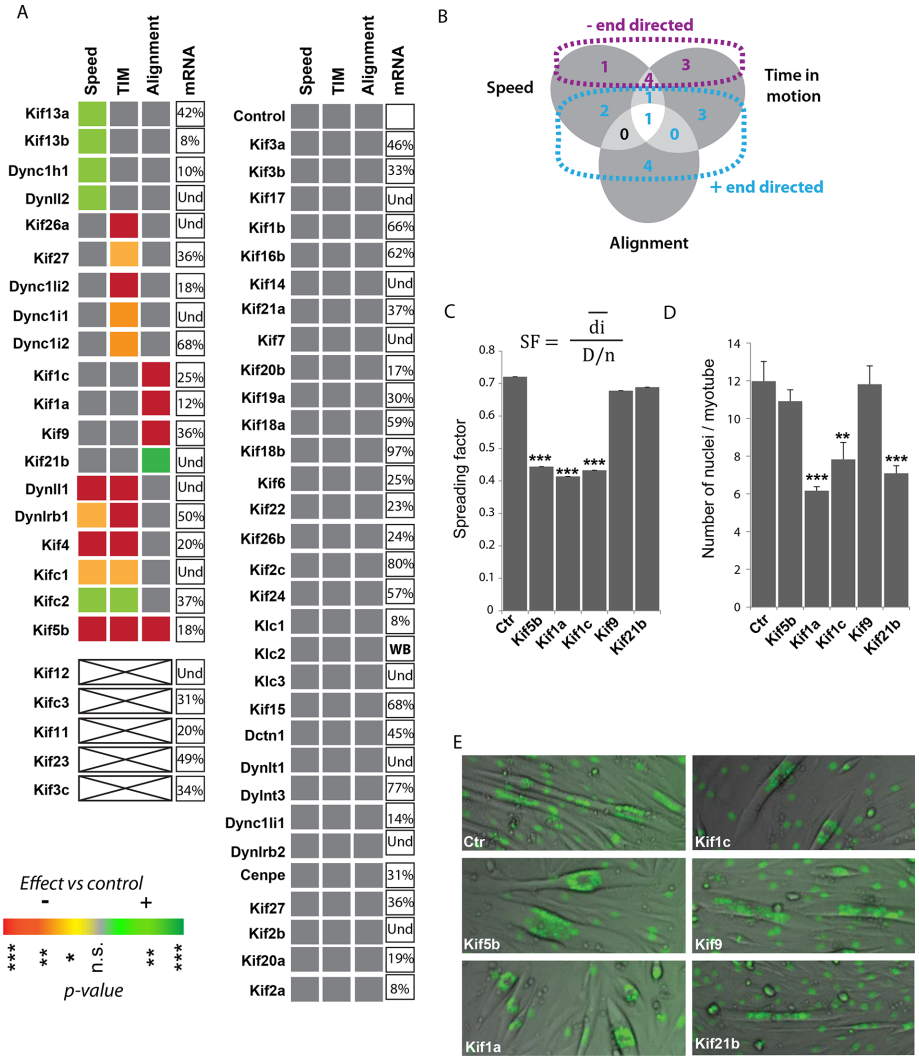

FIGURE 2: MT motor siRNA screen for nuclear movement and alignment in myotubes. (A) STA graph after silencing of kinesin or dynein members for nuclei inside myotubes after 3 d of differentiation. Colors are representative of the *p* values after one-way ANOVA statistical test toward a decrease (red) and increase (green) compared to control. ***$p < 0.001$, **$p < 0.01$, *$p < 0.05$. The percentage of remaining mRNA after silencing is also indicated. (B) Venn diagram to summarize the results obtained with siRNA screen, showing the distribution of genes implicated in one or more of the nuclear behaviors. Purple, proteins implicated in minus end–directed motion; blue, plus end–directed proteins. (C) Distribution of nuclei in myotubes and (D) number of nuclei per myotubes in five different conditions (Ctr, Kif5b, Kif1a, Kif1c, Kif9, and Kif21b siRNAs) after 88 h of differentiation. Spreading factor is the ratio between observed average distance and theoretical maximum distance between nuclei (41–76 myotubes). (E) Representative image of myotubes in each condition.

where nuclei inside myotubes move 55% of the time (±1.3) at a speed of 0.278 µm/min (± 0.1), similar to previously published results on nuclei speed (Figure 1C; Wilson and Holzbaur, 2012).

Nuclear movement and alignment are mainly MT dependent

We first investigated the contribution of actin and MT networks to nuclear behavior inside myotubes. Because these two networks are essential for fusion (Dobi *et al.*, 2011; Cadot *et al.*, 2012), we applied drugs affecting MTs (nocodazole and Taxol) and actin (cytochalasin D and jasplakinolide) 3 d after differentiation. After testing a range of concentrations, we used concentrations that did not affect global shape of myotubes but did impair cytoskeletal dynamics (Brown and Spudich, 1979; Schiff and Horwitz, 1980; Vasquez *et al.*, 1997; Bubb *et al.*, 2000; Rotsch and Radmacher, 2000). Surprisingly, some parameters, such as time in motion, are only slightly modified by actin-targeted drugs. Percentage of time in motion decreased from 55% in control to 34% in 25 nM cytochalasin D and to 45% in 200 nM jasplakinolide (Figure 1, A and D). However, other characteristics are more drastically affected, such as nuclei speed, which decreased to 0.20 µm/min in cytochalasin D– and 0.23 µm/min in jasplakinolide-treated myotubes, compared with 0.27 µm/min in controls (Figure 1C and Supplemental Movie S1). Of interest, drugs targeting the actin network did not affect the alignment of nuclei in myotubes (Figure 1C).

To hamper MT dynamics without affecting the overall shape of myotubes, we used drugs at low concentrations (75 nM nocodazole and 100 nM Taxol). Some parameters are highly modified during the first 24-h exposure, such as a dramatic decrease in the percentage of time in motion compared with control (Figure 1, A and D). Nuclear speed inside myotubes also decreases in nocodazole- and Taxol-treated myotubes (Figure 1C and Supplemental Movie S1A). To confirm MT involvement in maintaining these parameters, we overexpressed constitutively active spastin, a MT-severing protein (White *et al.*, 2007). We previously found that expression of spastin, but not the non–MT-severing mutant, prevents nuclear movement after fusion (Cadot *et al.*, 2012). We now found that ectopic expression of spastin in myotubes dramatically reduces nuclear motion and organization (Figure 1, B–D). To facilitate our readout, we represented the three measured parameters in an STA graph (speed, time in motion, and alignment), as represented in Figure 1E. These results describe the initial step of myofiber formation—when nuclei move extensively to establish an elongated myotube containing aligned nuclei. These results demonstrate the paramount role of dynamic MTs in nuclear movement within the myotube.

Identification of MT motors involved in nuclear spreading in myotubes

Next we sought to identify the MT-related molecular motors implicated in nuclear movement behavior. We performed an siRNA screen with three different sequences for each known kinesin and cytoplasmic dynein subunit (56 proteins; Table 1). STA parameters were measured in three different experiments on an area of 3.79 mm², corresponding to a single field of view under the microscope at a 4× magnification. We also quantified the fusion index to monitor the effect of protein silencing on the fusion process (Supplemental Figure S1C). At 36 h after silencing, cells were induced to differentiate into myotubes. Nuclear trajectories were analyzed

using SkyPad (Cadot *et al.*, 2014) from 60 to 75 h after the induction of differentiation (Supplemental Figure S2, A and B). At this time, the initial fusion events and their associated nuclear movements (centration) are terminated, and myotubes contain enough nuclei to be monitored for their displacements. The last frame of each movie was used to quantify nuclei alignment in myotubes and fusion index (Supplemental Figures S1C and S2C). The data were compiled in an STA graph, allowing an easy overview of the effect of all kinesins and dynein members on nuclear movement behavior (Figure 2A). In our conditions, cells divide at least once before differentiation. Therefore depletion of motors implicated in the cell division process leads to massive cell death: Kif11 (Eg5), which is an establisher of the bipolar spindle (Blangy *et al.*, 1995), Kif23 (MKLP-1), and Kif12, which is known to be essential for cytokinesis (Lakshmikanth *et al.*, 2004; Zhu *et al.*, 2005). Depletion of two other kinesins leads to failure in differentiation: Kifc3, responsible for Golgi positioning and integration (Xu *et al.*, 2002), and Kif3c, a kinesin whose function remains to be elucidated (Yang *et al.*, 2001). We were still able to quantify the fusion index for the remaining cells, but the nuclei number per myotube (two to five) was too low to allow correct quantification of the other STA parameters. Of interest, dynein motor inhibition does not lead to any gross cell fusion defects (Figure 2A and Supplemental Figure S1C). Furthermore, we did not find any correlation between defects in nuclei behavior and fusion index. For example, Kif5b or Kif20a depletion affects uniquely nuclear movement or fusion index, respectively. It is important to note that efficiency of knockdown might have affected the functional readouts. We therefore measured the percentage of remaining mRNA for most targets by Taqman (Figure 2A) or at the protein level by Western blot (Supplemental Figure S1B).

We found eight minus end–directed motors or associated proteins and 11 plus end–directed motors involved in at least one nuclear movement behavior (Figure 2B), suggesting a high degree of complexity for the regulation of nuclear positioning in muscle cells. Several motors affect only one nuclear behavior; depletion of members of the kinesin-3 family (Kif13a, Kif13b), the dynein heavy chain (Dync1h1), and the dynein light chain LC8-type2 (Dynll2) solely increase nuclear speed. Kif13a and Kif13b are mainly involved in endosome trafficking (Delevoye *et al.*, 2009, 2014). However, recent evidence demonstrated that the *Drosophila* homologue of Kif13b, khc73, is implicated, together with dynein heavy chain, in spindle positioning by anchoring MTs to the cell cortex (Lu and Prehoda, 2013). We previously showed that dynein is important in nuclear centration movement, probably through its localization at the nuclear envelope (Cadot *et al.*, 2012). In contrast, others found that depletion of dynein reduces nuclear speed in myotubes (Wilson and Holzbaur, 2012). These differences may stem from the fact that their measurements were done 168 h after differentiation, when nuclear movement characteristics (speed and percentage of time in motion) could be different from those in our analysis (60 h after differentiation). Because Dynll2 is involved in the formation of the dynein complex (Rapali *et al.*, 2011), its identification as playing a role in nuclear speed is in agreement with previous reports and emphasizes the connection between dynein and Kif13b.

The time in motion of nuclei was reduced exclusively after silencing of Kif26a, Kif27, Dync1i1, Dync1i2, or Dync1li2. Little is known about the function of Kif26a and Kif27, whereas Dync1i1, Dync1i2, and Dync1li2 are cargo adapters for dynein. Their absence could thus induce a delay in the recruitment of motors involved in moving the nucleus.

A few motors affect two types of nuclei behavior without altering others. Kif4 knockdown before differentiation leads to a decrease in speed and time in motion. Kif4 is known to be involved in the alignment of MTs in *Xenopus* (Mitchison *et al.*, 2013) and might have the same activity during myotube formation. Depletion of Kifc1, Kifc2, Dynlrb1, or Dynll1 affects both nuclei speed and time in motion but does not perturb nuclei alignment (Figure 2A). Kifc1, also known as HSET, is as a centrosome-clustering protein in cancers with supernumerary centrosomes (Chavali *et al.*, 2016) but is also capable of transporting the MT minus-end protein γ-tubulin (Lecland and Lüders, 2014). Because there is a relocalization of MT nucleation toward the nuclear envelope and a disappearance of centrosomes during differentiation (Tassin *et al.*, 1985), Kifc1 might affect these events and thereby perturb normal nuclear positioning.

Unexpectedly, knockdown of kinesin light chain 1, 2, or 3 did not effect nuclear movement or organization. As previously suggested, however, redundancy of Klc1 and 2 may require double knockdown of these proteins to observe an effect on nuclear aggregation (Wilson and Holzbaur, 2015).

As expected, only knockdown of the motor protein Kif5b altered the three types of nuclear behavior (Figure 2A). Kif5b was already implicated in nuclear rotation, movement, and positioning in muscle cells (Metzger *et al.*, 2012; Wilson and Holzbaur, 2012, 2015). Kif5b was also identified as the kinesin responsible for basally directing nuclear movement in neurons and thus contributing to neurogenesis (Tsai *et al.*, 2010).

Motors affecting nuclear alignment

Because nuclear alignment might depend on a complex mechanism, we decided to focus our attention on the five motor proteins whose depletion affects nuclei alignment: Kif5b, Kif1c, Kif1a, Kif9, and Kif21b. Kif9 couples centrosomes to nuclei (Tikhonenko *et al.*, 2013). Kif1a and Kif1c are mutated in spastic paraplegia (Caballero Oteyza *et al.*, 2014; Dor *et al.*, 2014; Citterio *et al.*, 2015), and Kif1a is associated with interkinetic nuclear movement in the developing brain (Tsai *et al.*, 2010; Carabalona *et al.*, 2016). Finally, Kif21b knockdown increases nuclear alignment in myotubes.

We therefore further analyzed these phenotypes by measuring the spreading factor, that is, the ratio between the average observed distances between nuclei and the theoretically optimal distance. We found a similar reduction of this ratio in Kif5b-, Kif1a-, and Kif1c-knockdown myotubes (Figure 2C). Unexpectedly, this factor was nearly unchanged in myotubes depleted for Kif9 or Kif21b. Kif9-silenced myotubes display aggregated nuclei, but the phenotype is different from the one observed in Kif5b- or Kif1a-depleted myotubes. In the kif9 siRNA cohort, nuclei form distinct clusters along the length of the myotube, yielding a higher average distance between nuclei than in Kif5b-knockdown myotubes (Figure 2, C and E, and Supplemental Figure S2D). Concerning Kif21b depletion, the increase in the percentage of myotubes with aligned nuclei does not imply an increase in nuclear spreading.

To understand whether these motors affect differentiation, we measured, besides the fusion index (Supplemental Figure S1CD), the number of nuclei per myotube, which represents myotube size (Figure 2D). Kif5b or Kif9 depletion shows an increase in the fusion index while maintaining a normal number of nuclei per myotube. This suggests that even if kif5b and kif9 affect nuclear positioning, they do not interfere with the myogenic program. On the other hand, Kif1a or Kif1c depletion does not affect the fusion index but affects the number of nuclei per myotube. The

most plausible explanation is that this result stems from a reduction in the number of cells available for fusion. Kif1a or Kif1c must therefore have an effect on the cycle of division before differentiation. Nevertheless, both motors remain interesting candidates for nuclear aggregation. Finally, Kif21b depletion decreases both the fusion index and the number of nuclei per myotube, suggesting a dual role, one for nuclear alignment and one for differentiation.

MT motors could affect nuclear movement and positioning by modifying MT organization or dynamics. To answer this question, we analyzed the orientation and length of EB1 comets in myotubes over a period of 200 s after depletion of a few motors (Supplemental Figure S1, D and E). This quantification of the MT growing plus ends allowed us to estimate the dynamics of the MTs and their organization. Most MTs grow parallel to the longest axis of the myotube (Supplemental Figure S1D). Only slight modifications in comet orientation were found after depletion of Kif5b or Dynlrb1, which could correlate with the observed differences in nuclear behavior. Surprisingly, the lengths of the EB1 comets were significantly modified after depletion of several motors without any correlation to their individual effects on nuclear movement (Supplemental Figure S1E). We hypothesize that normal nuclear movement might rely on different aspects—an oriented MT network, dynamic MTs, and molecular motors—to produce the necessary forces.

The nucleus represents the biggest organelle in the cell, and these findings illustrate the complexity required to move as well as organize the distribution of multiple nuclei in a large muscle cell. Several interesting candidates remain to be explored for their specific role, such as the proteins affecting two parameters of nuclear behavior. This opens new routes of research toward understanding intracellular organization.

MATERIALS AND METHODS

Cell line

C2C12 cells were cultured in DMEM with 10% fetal bovine serum (Invitrogen) and antibiotics (penicillin at 100 U/ml and streptomycin at 100 µg/ml) and were plated on 0.1% gelatin-coated dishes or acid-washed coverslips for 1–2 d before differentiation. Differentiation was induced by switching to DM (DMEM with 1% horse serum).

Chemicals and plasmids

Drugs were applied on 48-h-differentiated C2C12 cells and directly time-lapse recorded during 10 h. STA parameters were quantified during this time period. Taxol was from Calbiochem (580555), nocodazole from Sigma-Aldrich (M1404), cytochalasin D from Calbiochem (250255), and jasplakinolide from Santa Cruz Biotechnology (sc-202191A). YFP-Δ-227-spastin (C-terminus truncation) was a gift from Brett Lauring (Columbia University, New York).

siRNA transfection

Cells were transfected with three different siRNAs per gene using RNAiMAX, following the manufacturer's instructions (Life Technologies), 2 d before differentiation. For spastin cDNA transfection, we used Lipofectamine 2000 (Life Technologies), and cells were switched to DM 12 h after transfection. siRNAs were obtained from Life Technologies (primers used are listed in Table 1).

Microscopy

Epifluorescence images were acquired using a Nikon Ti microscope equipped with a CoolSNAP HQ2 camera (Roper Scientific) and an *XY*-motorized stage (Nikon) driven by MetaMorph (Molecular Devices). Multipositioning images were stitched with MetaMorph. For live imaging, we used an incubator to maintain cultures at 37°C and 5% CO_2 (Okolab).

Quantification of nuclear movement and positioning inside myotubes

We used the SkyPad algorithm as previously described (Cadot *et al.*, 2014) to quantify speed and time in motion. Briefly, nuclei centroids positions were manually picked every 15 min over 15 h, and coordinates were transferred to an Excel spreadsheet before running the SkyPad algorithm. For nuclear positioning, we identified three possible situations: nuclei are spread along the myotube axis (aligned), nuclei are clustered together (aggregated), and there is a mix of both (other). To calculate the spreading factor, we measured the nuclei interdistances and the length of the myotube. The spreading factor is the observed average interdistance over the optimal interdistance, that is, the myotube length divided by the number of nuclei.

Quantification of fusion index and number of nuclei per myotubes

The fusion index was calculated as percentage of nuclei found inside myotubes (more than two nuclei) over the total number of nuclei present in the same area (3.79 mm^2) at the end of each movie, 88 h after switching to differentiation medium.

Validation of siRNA knockdown by Western blot and reverse transcription quantitative PCR

At 48 h after silencing, cells were lysed in 1% SDS in phosphate-buffered saline (PBS) and passed through Qiashredder columns. Equal amounts of proteins were loaded on 4–12% gradient gels, followed by transfer on nitrocellulose membrane using the iBlot apparatus (Life Technologies). Primary antibodies were from Bethyl (Kif1b, Klc2), BD (Dcnt1), and Santa Cruz Biotechnology (kif5b). mRNAs from C2C12 cells were isolated with the RNeasy 96 Kit (Qiagen), and cDNA was prepared with the High-Capacity cDNA Reverse Transcription Kit (Life Technologies). Quantitative PCR (qPCR) analyses were performed using Taqman Gene Expression assay (Life Technologies; see Table 1) in a StepOne Plus system (Applied Biosystems). For Kif5b, Kif1a, and Kif26b, mRNAs from C2C12 cells were isolated with the RNeasy Micro Kit (Qiagen), and cDNA was prepared with the Transcriptor First-Strand cDNA Synthesis Kit (Roche). qPCR was performed using a CyberGreen Kit in a LightCycler 480 II system (Roche), using the following primers: Kif5b-F, 5′-GGAGGCAAGCAGTCGTAAAC-3′; Kif5b-R, 5′-TCTAGTGTTGGGAAGCAGCA-3′; Kif1a-F, 5′-GAAGACTCCCTCCCCTGTTC-3′, Kif1a-R, 5′-ATCTCTCCACCGTGTCCTTG-3′, Kif26b-F, 5′-TGGGGAACCATTCGAAATTA, Kif26b-R, 5′-AGGACCTGCTCCAAGTCAAA-3′; Hprt1-F, 5′-GTTAAGCAGTACAGCCCCAAA-3′; and Hprt1-R, 5′-AGGGCATATCCAACAACAAACTT-3′.

Statistics

A Gaussian distribution of averaged speeds of each nucleus was tested using the D'Agostino and Pearson omnibus normality test for each condition (GraphPad software); it appeared that the distribution was not Gaussian, and so the statistical significance between conditions was measured using the Mann–Whitney test for non-Gaussian distributions. A normal Student's *t* test was used otherwise.

RefSeq accession number	Gene symbol	Sense siRNA sequence	Antisense siRNA sequence	Taqman assay ID
NM_008440	Kif1a	GGACAUCAACUAUGCCUCUtt GGAAACAGAGAAGAUCAUUtt CCAAGUCCUUCAUCGAAUAtt	AGAGGCAUAGUUGAUGUCCtc AAUGAUCUUCUCUGUUUCCtt UAUUCGAUGAAGGACUUGGtc	Mm00492863_m1
NM_207682	Kif1b	CGGGCUGAUUCAACUGGUGtt CCUCAAUGAAGACCCAUUAtt GGAUGGAAUUACAAGGGUUtt	CACCAGUUGAAUCAGCCCGtt UAAUGGGUCUUCAUUGAGGtt AACCCUUGUAAUUCCAUCCtt	Mm00801827_m1
NM_153103	Kif1c	CCUUCGACUAUUCUUACUGtt GGAAACAGAGAAGAUCAUAtt CCAUGUUUUCCGCUUCAAUtt	CAGUAAGAAUAGUCGAAGGtg UAUGAUCUUCUCUGUUUCCtg AUUGAAGCGGAAAACAUGGtt	Mm00462184_m1
NM_008442	Kif2a	GGGAAUUUAUGCAUUAGCAtt CGCAGAUCAAUUUUCAUAGtt GCUCCUAAUGAAAUGGUUUtt	UGCUAAUGCAUAAAUUCCCtt CUAUGAAAAUUGAUCUGCGtt AAACCAUUUCAUUAGGAGCtg	Mm00515233_m1
NM_134471	Kif2c	GGAGGUACCACAAAAGGCAtt GGCAAAGAGAUUGACAUUGtt GCAGAAAUUAACAAGUCUCtt	UGCCUUUUGUGGUACCUCCtt CAAUGUCAAUCUCUUUGCCtt GAGACUUGUUAAUUUCUGCtc	Mm00728630_s1
NM_008443	Kif3a	GGGCGACACAAGGUUUUUGtt GGGACCAAGCAGGUAAAAAtt CCGUAAUUGAUUCUUUACUtt	CAAAAACCUUGUGUCGCCCtc UUUUUACCUGCUUGGUCCCtt AGUAAAGAAUCAAUUACGGtc	Mm01288585_m1
NM_008444	Kif3b	GGAUUUGUCUUCUUUUGUCtt GGUGGUAGAUGCGGAUGUGtt GGGUUUCAAUGGCACAAUUtt	GACAAAAGAAGACAAAUCCtt CACAUCCGCAUCUACCACCtt AAUUGUGCCAUUGAAACCCtg	Mm00492891_m1
NM_008445	Kif3c	GGAGAAUCCUGAAACAGGGtt GGAAGAUGAUAACAACAACtt CCGGCUAUCUUUGAGAUGGtt	CCCUGUUUCAGGAUUCUCCtt GUUGUUGUUAUCAUCUUCCtc CCAUCUCAAAGAUAGCCGGtg	Mm00492900_m1
NM_008446	Kif4	GGUGGUGGUUGGUAAUGAUtt GGAAGAGGUCUUUAAUACAtt GGAUACAAUGCAACUGUCCtt	AUCAUUACCAACCACCACCtg UGUAUUAAAGACCUCUUCCtg GGACAGUUGCAUUGUAUCCtt	Mm00492908_m1
NM_177052	Kif6	CCUGGCAGAUGGAUUCGUAtt GCUUCAACCCGGUCACACUtt CGAAUGUGGCUAUGACCUGtt	UACGAAUCCAUCUGCCAGGtc AGUGUGACCGGGUUGAAGCtt CAGGUCAUAGCCACAUUCGtt	Mm00723857_m1
NM_010628	Kif9	GGACUUGGUUUAUGAAACAtt GCAUCGACAUCCACUUGAAtt GGCUUGUCAGUGCAUCUCAtt	UGUUUCAUAAACCAAGUCCtg UUCAAGUGGAUGUCGAUGCtt UGAGAUGCACUGACAAGCCtt	Mm00495130_m1
NM_010615	Kif11	CCAUUUAAUCUGGCAGAGCtt GCUUGUUAAAAUUGGAAAGtt GGUCUACUGAUAUAAUCAAtt	GCUCUGCCAGAUUAAAUGGtc CUUUCCAAUUUUAACAAGCtc UUGAUUAUAUCAGUAGACCtc	Mm01204225_m1
NM_010616	Kif12	CCUGGCUAUUAGAUCGCGUtt CCUGAGUCUCGGUUCACAAtt CCUUCACCUGGCUAUUAGAtt	ACGCGAUCUAAUAGCCAGGtg UUGUGAACCGAGACUCAGGtt UCUAAUAGCCAGGUGAAGGtc	Mm00802885_m1
NM_010617	Kif13a	GGUAUCGUAUAUGGAGAUCtt GGGAAAUAAGUCUCGAACGtt GCUGGAGAAUAAGCUAAUUtt	GAUCUCCAUAUACGAUACCtc CGUUCGAGACUUAUUUCCCtc AAUUAGCUUAUUCUCCAGCtt	Mm00660179_m1
NM_010620	Kif15	GGAGUCUGUAUUCUCAACAtt GCGGUUAUAAUGGGACCAUtt GCAAACCUCAAUCUUGAAAtt	UGUUGAGAAUACAGACUCCtg AUGGUCCCAUUAUAACCGCtc UUUCAAGAUUGAGGUUUGCtt	Mm01341275_m1

TABLE 1: siRNA sequences and Taqman probes used for each molecular motor.

Continues

RefSeq accession number	Gene symbol	Sense siRNA sequence	Antisense siRNA sequence	Taqman assay ID
NM_010623	Kif17	GGCAGUGGGAAGUCUUUCAtt GGAGGCCACCAAAAUUAACtt CCCUGAUGAAUAAGGACUCtt	UGAAAGACUUCCCACUGCCtg GUUAAUUUUGGUGGCCUCCtt GAGUCCUUAUUCAUCAGGGtg	Mm00456740_m1
NM_139303	Kif18a	GGCGGUGCAGUUCUGUAAAtt GCCAAUCCUUCAUAGUUUUtt CGUGCUUAAACUUACUCCAtt	UUUACAGAACUGCACCGCCtt AAAACUAUGAAGGAUUGGCtt UGGAGUAAGUUUAAGCACGtt	Mm01327661_m1
NM_028547	Kif2b	CCAAUGAACUAGUUUACCATT CGACAAUACGAAUUCGGGATT GCUCCAAUCACUACGAGAATT	UGGUAAACUAGUUCAUUGGAT UCCCGAAUUCGUAUUGUCGTT UUCUCGUAGUGAUUGGAGCTT	Mm01308520_s1
NM_010626	Kif7	GGAGAACGGCUCAAAGAGATT GCCUGGAGAUUGAUAGCAATT CAACAGCAAAAGAUCCUGATT	UCUCUUUGAGCCGUUCUCCGG UUGCUAUCAAUCUCCAGGCGT UCAGGAUCUUUUGCUGUUGCT	Mm01320530_m1
NM_001081177	Kif13b	AGACGGGCAUUGUACGGUATT GGCUAGAAGUAACAUCUGATT CCAUCUCCCAUGGUGGUUATT	UACCGUACAAUGCCCGUCUTG UCAGAUGUUACUUCUAGCCTC UAACCACCAUGGGAGAUGGAG	Mm01314840_m1
NM_001081258	Kif14	CAGGGAUGCUGUUCGGAUATT CCUCUGUUCGAGUUCGUAATT GGAAAGUCCUAUACGAUGATT	UAUCCGAACAGCAUCCCUGCA UUACGAACUCGAACAGAGGTA UCAUCGUAUAGGACUUUCCAG	Not available
NM_001081133	Kif16b	GUACAUAAUUCAACAUAUATT CACUUAGAGAAAUACCUCATT GGAUUUGGAUUUAAUAAUATT	UAUAUGUUGAAUUAUGUACAT UGAGGUAUUUCUCUAAGUGTG UAUUAUUAAAUCCAAAUCCAA	Mm01327880_m1
NM_001102615	Kif19a	GAAGGAGUCCUACACCAAATT CAACUAUCGGGACAGCAAATT CAAUCUAUCUAGCAGCACATT	UUUGGUGUAGGACUCCUUCCT UUUGCUGUCCCGAUAGUUGAT UGUGCUGCUAGAUAGAUUGTC	Mm01244862_m1
NM_183046	Kif20b	CAACGGUAGAAGUAAGUAATT CCAACGAUCUAAGUGCAAATT GCGAAUAAUUUGCAUGAUATT	UUACUUACUUCUACCGUUGAT UUUGCACUUAGAUCGUUGGTT UAUCAUGCAAAUUAUUCGCCA	Mm01205010_m1
NM_001097621	Kif26a	UGACGAGUUUGAUGCUUAUTT GCCCUGAACGUAUGUCGAATT AGAUCAAGGUGUACGAAAUTT	AUAAGCAUCAAACUCGUCATT UUCGACAUACGUUCAGGGCCT AUUUCGUACACCUUGAUCUCA	Mm01339746_m1
NM_009004	Kif20a	GGACCUGUUGUCAGACUGCtt GGUGAAAGUUUACCUUCGAtt CGUACACCAUUCAAGGUACtt	GCAGUCUGACAACAGGUCCtt UCGAAGGUAAACUUUCACCtt GUACCUUGAAUGGUGUACGtt	Mm00436226_m1
NM_016705	Kif21a	GGAUAUUGCCAGUAAUUAAtt CCCAGUGCAUCGAAAAGCUtt CGAAGAGAUCAGUAAUAUGtt	UUAAUUACUGGCAAUAUCCtc AGCUUUUCGAUGCACUGGGtg CAUAUUACUGAUCUCUUCGtt	Mm00497322_m1
NM_019962	Kif21b	GGAAAAAGUUCCAAAAGAAtt GGAGAAGAUGCUGUCUUGCtt GGCUGCUCAAAAAGAACAUtt	UUCUUUUGGAACUUUUUCCtg GCAAGACAGCAUCUUCUCCtt AUGUUCUUUUUGAGCAGCCtg	Not available
NM_145588	Kif22	GGAAGUCUAUGUAGGUUCAtt GGGCAGAAUGCCAGUGUACtt GGAAAACUCUACCUUAUUGtt	UGAACCUACAUAGACUUCCtg GUACACUGGCAUUCUGCCCtt CAAUAAGGUAGAGUUUUCCtt	Mm01139072_m1
NM_024245	Kif23	GGGCUAUCGACUCAACAGAtt GGAAAAAGAGCAAAUUACUtt GCAUAGGGUCAUUUCAAGCtt	UCUGUUGAGUCGAUAGCCCtc AGUAAUUUGCUCUUUUUCCtg GCUUGAAAUGACCCUAUGCtg	Mm00458527_m1

TABLE 1: siRNA sequences and Taqman probes used for each molecular motor.

Continues

RefSeq accession number	Gene symbol	Sense siRNA sequence	Antisense siRNA sequence	Taqman assay ID
NM_024241	Kif24	GCCAAGAGGACAUUUGGCAtt CCAGCAUUCACCUGACAAAtt GCAUGUGGUACAGAUAGCUtt	UGCCAAAUGUCCUCUUGGCtg UUUGUCAGGUGAAUGCUGGtg AGCUAUCUGUACCACAUGCtt	Mm01211351_m1
NM_177757	Kif26b	GGAGAGAGAUGAAAUUUGAtt CCUUCGAGACCUGUUGUCUtt GCUCUCAGCAAAAACCGAGtt	UCAAAUUUCAUCUCUCUCCtt AGACAACAGGUCUCGAAGGtt CUCGGUUUUUGCUGAGAGCtt	Not available
NM_175214	Kif27	GGAUCUCUACUUCUAUAAGtt GGCCAUGUUGCAUCAGUUGtt	CUUAUAGAAGUAGAGAUCCtt CAACUGAUGCAACAUGGCCtc	Mm00723524_m1
NM_053173	Kifc1	GGCUAAUAAGAAGUGAAGUtt GGAACUGAAGGGCAAUAUCtt GGCCAUUAACAGCAGUCUGtt	ACUUCACUUCUUAUUAGCCtg GAUAUUGCCCUUCAGUUCCtg CAGACUGCUGUUAAUGGCCtg	Mm03011779_m1
NM_010630	Kifc2	GGAGGAACAGAGAGUUUGGtt GGUCAACCUUUAAAAAACAtt GCUGAGUAGACUUCGUCUGtt	CCAAACUCUCUGUUCCUCCtc UGUUUUUUAAAGGUUGACCtg CAGACGAAGUCUACUCAGCtc	Mm00495161_m1
NM_010631	Kifc3	GGGCAUGUAUAUAAUGUUCtt CGACUACAAUGGGCUCAAGtt GGUUAAUAGCAACAACCAGtt	GAACAUUAUAUACAUGCCCtg CUUGAGCCCAUUGUAGUCGtt CUGGUUGUUGCUAUUAACCtc	Mm00516085_m1
NM_008451	Klc2	GGCGGUGAUCCAGGGUUUAtt GGGUUUAGAGACCCUGAGAtt GGUGGUAGAACUGUUAAAAtt	UAAACCCUGGAUCACCGCCtt UCUCAGGGUCUCUAAACCCtg UUUUAACAGUUCUACCACCtt	Mm00492945_m1
NM_146182	Klc3	CAAAUGUGGCCAAGACUAAtt GGAGGCUAGCCCAAGAGAAtt AUGGAAAACGUGGACGUUAtt	UUAGUCUUGGCCACAUUUGgg UUCUCUUGGGCUAGCCUCCgt UAACGUCCACGUUUUCCAUag	Mm00461422_m1
NM_001025360	Klc1	GGAGGAGAAGAAACACCUGtt CCUAGCAGUACUGUACGGUtt GGGAUCAGAACAAGUAUAAtt	CAGGUGUUUCUUCUCCUCCtc ACCGUACAGUACUGCUAGGtt UUAUACUUGUUCUGAUCCCtg	Mm00492936_m1
NM_197959	Kif18b	CGAGCGGAUGCUGGUAUUUtt GCCGAGCAGUUACUUGAGAtt CCUACGAGGAUACUUACAAtt	AAAUACCAGCAUCCGCUCGtc UCUCAAGUAACUGCUCGGCtg UUGUAAGUAUCCUCGUAGGtc	Mm01253048_g1
NM_173762	Cenpe	GGUUCAAGAACUUAAGACAtt GGAAAUGCUCAAAGAUUUUtt GGAUUACUGAUCUCCAAAAtt	UGUCUUAAGUUCUUGAACCtt AAAAUCUUUGAGCAUUUCCtc UUUUGGAGAUCAGUAAUCCtt	Mm00620549_m1
NM_030238	Dync1h1	GGAGAAAGAAUUCAUUUCCtt GCUCCUGUGAUUGAUGCAGtt GGAGGUUAUGUUUAAAACUtt	GGAAAUGAAUUCUUUCUCCtc CUGCAUCAAUCACAGGAGCtc AGUUUUAAACAUAACCUCCtc	Mm00466548_m1
NM_010063	Dync1i1	GGAAGAGGAGAGGAAGAAGtt CCCAAAAUUGGUCAUGAUUtt GGAAGAAAAACAGCAGAUCtt	CUUCUUCCUCUCCUCUUCCtt AAUCAUGACCAAUUUUGGGtt GAUCUGCUGUUUUUCUUCCtc	Mm01135515_m1
NM_010064	Dync1i2	CCAUUCUACGAGAAUUGUAtt GCAGAUUAACAUCUUCUUUtt GGAAAGGAAAAAAAAGGAAtt	UACAAUUCUCGUAGAAUGGtc AAAGAAGAUGUUAAUCUGCtc UUCCUUUUUUUUCCUUUCCtc	Mm01333946_m1
NM_007835	Dctn1	CCACAUCAAGUUCACCCAGtt GGAAGUAUUUCACAUGUGAtt CCUGGAAACAUCAUGUAGUtt	CUGGGUGAACUUGAUGUGGtc UCACAUGUGAAAUACUUCCtt ACUACAUGAUGUUUCCAGGtc	Mm01184845_m1
NM_019682	Dynll1	GGAGUUUGACAAGAAGUACtt GGUGGCCAUUCUUCUGUUCtt GGACUGCAUCCAAAUUCCAtt	GUACUUCUUGUCAAACUCCtt GAACAGAAGAAUGGCCACCtg UGGAAUUUGGAUGCAGUCCtt	Mm00850282_g1

TABLE 1: siRNA sequences and Taqman probes used for each molecular motor.

Continues

RefSeq accession number	Gene symbol	Sense siRNA sequence	Antisense siRNA sequence	Taqman assay ID
NM_009342	dynlt1	GGAACCACAUGACUUCAGCtt GGCAGUACCACUUGUCUUAtt GGUGCUAAAAACUCAAGUCtt	GCUGAAGUCAUGUGGUUCCtg UAAGACAAGUGGUACUGCCtg GACUUGAGUUUUUAGCACCtt	Not available
NM_025975	Dynlt3	GCAUAGUGGAACAGUCUAUtt GGCCAUUAACUUAAGUUUGtt GCCCGUAUGGAUUUCACACtt	AUAGACUGUUCCACUAUGCtt CAAACUUAAGUUAAUGGCCtt GUGUGAAAUCCAUACGGGCtc	Mm00458834_m1
NM_025947	Dynlrb1	CCUUCCUUCGAAUUCGCUCtt GGCUUUGGAAUGAGAGCUUtt GGCAUUCCCAUCAAGAGCAtt	GAGCGAAUUCGAAGGAAGGtt AAGCUCUCAUUCCAAAGCCtg UGCUCUUGAUGGGAAUGCCtt	Mm00508951_m1
NM_026556	Dynll2	GGCCAUGGAGAAGUACAACtt GGACAUUGCUGCCUAUAUCtt GGUCUGAAGUAUAGCAAUGtt	GUUGUACUUCUCCAUGGCCtg GAUAUAGGCAGCAAUGUCCtt CAUUGCUAUACUUCAGACCtg	Not available
NM_029297	dylnrb2	GGAAUAUCUUCUGAUUGUCtt CGAAUCCAUGAUAUUGUACtt CGACCUGACUUUUCUUAGGtt	GACAAUCAGAAGAUAUUCCtt GUACAAUAUCAUGGAUUCGtg CCUAAGAAAAGUCAGGUCGtt	Mm00466467_m1
NM_146229	dync1li1	CCGGCUAAGAAAGACAAUUtt GCUACAGUCUCUUUUAGCAtt GCCUUGGACUGCUUUGGAUtt	AAUUGUCUUUCUUAGCCGGtc UGCUAAAAGAGACUGUAGCtt AUCCAAAGCAGUCCAAGGCtt	Mm01353886_m1
NM_001013380	dync1li2	GCAGGUUAAGUAGCUGACAtt CGUGCUGACUCAUAACCUGtt CGUAGCACUUCUUCUCUUAtt	UGUCAGCUACUUAACCUGCtt CAGGUUAUGAGUCAGCACGtt UAAGAGAAGAAGUGCUACGtt	Dync1li2

TABLE 1: siRNA sequences and Taqman probes used for each molecular motor. Continued

ACKNOWLEDGMENTS

We thank members of the Gomes lab for helpful discussions and W. Roman for correcting the manuscript. B.C. was supported initially by a Fondation pour la Recherche Médicale fellowship. V.G. was supported initially by a Region Ile-de-France fellowship. This work was supported by Muscular Dystrophy Association, INSERM Avenir Programme, and Agence Nationale de la Recherche grants to E.R.G. and Association Institut de Myologie and Agence Nationale de la Recherche grants to B.C.

REFERENCES

Abmayr SM, Pavlath GK (2012). Myoblast fusion: lessons from flies and mice. Development 139, 641–656.

Blangy A, Lane HA, d' Hérin P, Harper M, Kress M, Nigg EA (1995). Phosphorylation by p34cdc2 regulates spindle association of human Eg5, a kinesin-related motor essential for bipolar spindle formation in vivo. Cell 83, 1159–1169.

Brown SS, Spudich JA (1979). Cytochalasin inhibits the rate of elongation of actin filament fragments. J Cell Biol 83, 657–662.

Bruusgaard JC, Liestøl K, Ekmark M, Kollstad K, Gundersen K (2003). Number and spatial distribution of nuclei in the muscle fibres of normal mice studied in vivo. J Physiol 551, 467–478.

Bubb MR, Spector I, Beyer BB, Fosen KM (2000). Effects of jasplakinolide on the kinetics of actin polymerization an explanation for certain in vivo observations. J Biol Chem 275, 5163–5170.

Caballero Oteyza A, Battaloğu E, Ocek L, Lindig T, Reichbauer J, Rebelo AP, Gonzalez MA, Zorlu Y, Ozes B, Timmann D, *et al.* (2014). Motor protein mutations cause a new form of hereditary spastic paraplegia. Neurology 82, 2007–2016.

Cadot B, Gache V, Gomes ER (2014). Fast, multi-dimensional and simultaneous kymograph-like particle dynamics (SkyPad) analysis. PLoS One 9, e89073.

Cadot B, Gache V, Vasyutina E, Falcone S, Birchmeier C, Gomes ER (2012). Nuclear movement during myotube formation is microtubule and dynein dependent and is regulated by Cdc42, Par6 and Par3. EMBO Rep 13, 741–749.

Carabalona A, Hu DJ-K, Vallee RB (2016). KIF1A inhibition immortalizes brain stem cells but blocks BDNF-mediated neuronal migration. Nat Neurosci 19, 253–262.

Chavali PL, Chandrasekaran G, Barr AR, Tátrai P, Taylor C, Papachristou EK, Woods CG, Chavali S, Gergely F (2016). A CEP215-HSET complex links centrosomes with spindle poles and drives centrosome clustering in cancer. Nat Commun 7, 11005.

Citterio A, Arnoldi A, Panzeri E, Merlini L, D'Angelo MG, Musumeci O, Toscano A, Bondi A, Martinuzzi A, Bresolin N, Bassi MT (2015). Variants in KIF1A gene in dominant and sporadic forms of hereditary spastic paraparesis. J Neurol 262, 2684–2690.

Dauer WT, Worman HJ (2009). The nuclear envelope as a signaling node in development and disease. Dev Cell 17, 626–638.

Delevoye C, Hurbain I, Tenza D, Sibarita J-B, Uzan-Gafsou S, Ohno H, Geerts WJC, Verkleij AJ, Salamero J, Marks MS, Raposo G (2009). AP-1 and KIF13A coordinate endosomal sorting and positioning during melanosome biogenesis. J Cell Biol 187, 247–264.

Delevoye C, Miserey-Lenkei S, Montagnac G, Gilles-Marsens F, Paul-Gilloteaux P, Giordano F, Waharte F, Marks MS, Goud B, Raposo G (2014). Recycling endosome tubule morphogenesis from sorting endosomes requires the kinesin motor KIF13A. Cell Rep 6, 445–454.

Dobi KC, Metzger T, Baylies MK (2011). Characterization of early steps in muscle morphogenesis in a Drosophila primary culture system. Fly (Austin) 5, 68–75.

Dor T, Cinnamon Y, Raymond L, Shaag A, Bouslam N, Bouhouche A, Gaussen M, Meyer V, Durr A, Brice A, *et al.* (2014). KIF1C mutations in two families with hereditary spastic paraparesis and cerebellar dysfunction. J Med Genet 51, 137–142.

Englander LL, Rubin LL (1987). Acetylcholine receptor clustering and nuclear movement in muscle fibers in culture. J Cell Biol 104, 87–95.

Falcone S, Roman W, Hnia K, Gache V, Didier N, Lainé J, Auradé F, Marty I, Nishino I, Charlet-Berguerand N, *et al.* (2014). N-WASP is required for amphiphysin-2/BIN1-dependent nuclear positioning and triad organization in skeletal muscle and is involved in the pathophysiology of centronuclear myopathy. EMBO Mol Med 6, 1455–1475.

Gundersen GG, Worman HJ (2013). Nuclear positioning. Cell 152, 1376–1389.
Jungbluth H, Wallgren-Pettersson C, Laporte J (2008). Centronuclear (myotubular) myopathy. Orphanet J Rare Dis 3, 26.
Lakshmikanth GS, Warrick HM, Spudich JA (2004). A mitotic kinesin-like protein required for normal karyokinesis, myosin localization to the furrow, and cytokinesis in Dictyostelium. Proc Natl Acad Sci USA 101, 16519–16524.
Lecland N, Lüders J (2014). The dynamics of microtubule minus ends in the human mitotic spindle. Nat Cell Biol 16, 770–778.
Lu MS, Prehoda KE (2013). A NudE/14-3-3 pathway coordinates dynein and the kinesin Khc73 to position the mitotic spindle. Dev Cell 26, 369–380.
Metzger T, Gache V, Xu M, Cadot B, Folker ES, Richardson BE, Gomes ER, Baylies MK (2012). MAP and kinesin-dependent nuclear positioning is required for skeletal muscle function. Nature 484, 120–124.
Mitchison TJ, Nguyen P, Coughlin M, Groen AC (2013). Self-organization of stabilized microtubules by both spindle and midzone mechanisms in Xenopus egg cytosol. Mol Biol Cell 24, 1559–1573.
Rapali P, Szenes Á, Radnai L, Bakos A, Pál G, Nyitray L (2011). DYNLL/LC8: a light chain subunit of the dynein motor complex and beyond. FEBS J 278, 2980–2996.
Rotsch C, Radmacher M (2000). Drug-induced changes of cytoskeletal structure and mechanics in fibroblasts: an atomic force microscopy study. Biophys J 78, 520–535.
Schiff PB, Horwitz SB (1980). Taxol stabilizes microtubules in mouse fibroblast cells. Proc Natl Acad Sci USA 77, 1561–1565.
Tassin AM, Maro B, Bornens M (1985). Fate of microtubule-organizing centers during myogenesis in vitro. J Cell Biol 100, 35–46.
Tikhonenko I, Magidson V, Graf R, Khodjakov A, Koonce MP (2013). A kinesin-mediated mechanism that couples centrosomes to nuclei. Cell Mol Life Sci 70, 1285–1296.
Tsai J-W, Lian W-N, Kemal S, Kriegstein A, Vallee RB (2010). An unconventional kinesin and cytoplasmic dynein are responsible for interkinetic nuclear migration in neural stem cells. Nat Neurosci 13, 1463–1471.
Vasquez R, Howell B, Yvon A, Wadsworth P, Cassimeris L (1997). Nanomolar concentrations of nocodazole alter microtubule dynamic instability in vivo and in vitro. Mol Biol Cell 8, 973–985.
White SR, Evans KJ, Lary J, Cole JL, Lauring B (2007). Recognition of C-terminal amino acids in tubulin by pore loops in Spastin is important for microtubule severing. J Cell Biol 176, 995–1005.
Wilson MH, Holzbaur ELF (2012). Opposing microtubule motors drive robust nuclear dynamics in developing muscle cells. J Cell Sci 125, 4158–4169.
Wilson MH, Holzbaur ELF (2015). Nesprins anchor kinesin-1 motors to the nucleus to drive nuclear distribution in muscle cells. Development 142, 218–228.
Xu Y, Takeda S, Nakata T, Noda Y, Tanaka Y, Hirokawa N (2002). Role of KIFC3 motor protein in Golgi positioning and integration. J Cell Biol 158, 293–303.
Yang Z, Roberts EA, Goldstein LS (2001). Functional analysis of mouse kinesin motor Kif3C. Mol Cell Biol 21, 5306–5311.
Zhu C, Bossy-Wetzel E, Jiang W (2005). Recruitment of MKLP1 to the spindle midzone/midbody by INCENP is essential for midbody formation and completion of cytokinesis in human cells. Biochem J 389, 373–381.